A new data reduction approach for the Clementine NIR data set: Application to Aristillus, Aristarchus and Kepler

Stéphane Le Mouélic, Yves Langevin, Stéphane Erard

JOURNAL OF GEOPHYSICAL RESEARCH, VOL. 104, NO. E2, PAGES 3833-3843, FEBRUARY 25, 1999

A new data reduction approach for the Clementine NIR data set: Application to Aristillus, Aristarchus and Kepler

Stéphane Le Mouélic, Yves Langevin, and Stéphane Erard

Institut d'Astrophysique Spatiale, Orsay, France

Abstract. The Clementine spacecraft, launched in January 1994, has performed a nearly global surface mapping of the moon in eleven broad spectral bands at a resolution of ~200 m. The UV-visible (UV/VIS) camera performed observations in five bands ranging from 0.415 to 1.0 μm, while the near infrared camera (NIR) acquired data in six spectral bands ranging from 1.1 to 2.78 μm. UV/VIS images are calibrated to ~4%. The calibrated NIR data set is yet to be finalized due to instrumental problems. Independently of the calibration effort for the full data set which is under the responsibility of the PI team, we present here the first results of a heuristic approach to extract mineralogical information from raw images in regions of particular interest. We processed images of craters Aristillus, Aristarchus, and Kepler. We computed band ratios using 0.75, 0.9, 0.95, 1.0, 1.1, 1.25, 1.5, and 2.0 μm images to map the compositional heterogeneity and to discriminate between pyroxene, olivine, or feldpar rich areas. Absolute reflectance spectra have been derived using telescopic spectra as ground truth. High orthopyroxene and clinopyroxene contents have been detected and spatially mapped on Aristillus. Our results are in good agreement with previous studies in the case of Aristarchus and show additional details due to the improved registration. Two regions exhibit spectra consistent with a high proportion of olivine with <25% pyroxene. The rim of Kepler exhibits a strong feature at 2 μm correlated with the 1 μm feature, suggesting either a high orthopyroxene content or a very immature soil. Our method could be of interest for further investigations of the lunar surface using Clementine NIR data.

1. Introduction

The Clementine spacecraft was launched in January 1994. It provided the first near global coverage of the lunar surface in a selected number of wavelenghs, which were chosen for their mineralogical interest [*Nozette et al.*, 1994]. More than one million images of the Moon, Earth and dark sky have been returned by this mission. The spatial resolution ranges from 100 meters per pixel at periselene to 400 meters per pixel at the poles. Two multispectral cameras were used for the surface mapping. The UV/VIS camera had filters at 450, 750, 900, 950, and 1000 nm and has led to significant improvements in our knowledge of the lunar soil mineralogy. The first global digital map of the Moon has been computed with a resolution of 100 meters per pixel by mosaicking images at 750 nm [*Isbell et al.*, 1997]. The near infrared camera (NIR) was designed to acquire images in six bands. Filters at 1.10, 1.25, 1.50, 2.00, 2.60, and 2.78 μm were chosen in order to complete the coverage of critical parts of common lunar minerals spectra. A large dark frame signal, which varies with time in the orbit, as well as gain and offset values uncertainties makes a global NIR calibration scheme very hard to achieve [*Priest et al.*, 1995]. The whole calibration process is currently being worked out with the support of NASA for the overall data set [*Lucey et al.*, 1997, 1998]. Independently of this whole data set reduction effort, we present here a heuristic approach which is aimed at evaluating the scientific potential of the NIR data set. In this paper, we restricted our investigations to the Aristillus, Aristarchus, and Kepler craters. These three craters were chosen for their geological interest, since other studies have demonstrated their spectral variability. Furthermore, they are all located at low to mid northern latitudes, so that the instrument temperatures were similar. This limits the changes in instrumental behavior which are observed along the orbit as the instrument warms up. Our approach is based on the relatively small variations of lunar red to near-IR spectra when compared to changes in illumination conditions and average albedo. At first order, the NIR data is therefore linearly correlated with the UV/VIS data, for which a reliable reduction scheme is available. This can be used to evaluate offsets and to derive normalized images for each of the IR bands. Ratios of normalized IR bands were computed to map the spatial extent of the major spectral heterogeneities. Spectra were extracted from these regions and were calibrated using telescopic spectra as ground truth. After presenting the selected data set, we will discuss the main systematic effects that are to be removed from the NIR images. Then, the processing steps and the verification means will be defined. The method

Paper number 1998JE900035.
0148-0227/99/1998JE00035$09.00

will finally be applied to our selected areas, demonstrating that the computed band ratios and extracted spectra from the NIR data set provide reliable information on the mineralogical diversity of the lunar surface.

2. Data Selection

The mineralogy of the lunar surface is mostly dominated by feldspar, pyroxene, olivine, and ilmenite. Glasses and impact melts derived from these mineral species are also abundant. Reviews of the mineralogical composition of the lunar regolith are given by *McKay et al.* [1991] and *Pieters* [1986]. Laboratory spectra of pure minerals, as well as mixtures, have been measured [*Singer,* 1981; *Cloutis and Gaffey,* 1993; *Crown and Pieters,* 1987]. Laboratory spectra of the four main lunar mineral species are displayed in Figure 1, superimposed on the Clementine filters used in this study. Although several parameters such as grain size, maturity, or mixing rates modify the observed spectra, laboratory studies are of great interest for the interpretation of the data.

We selected four of the six spectral bands from the NIR data set according to image quality and mineralogical interest: the 1100, 1250, and 2000 nm bands are good indicators of olivine, feldspar, and orthopyroxene, respectively, and permit discrimination between these three mineral species. The 1500 nm band has been used to define a continuum level (see Figure 1). Images at 2600 nm have a lower signal to noise ratio, and the signal at 2780 nm has a thermal emission contribution; therefore they were not used in the present study.

We selected four of the five spectral bands in the UV/VIS domain in order to compare our interpretation of the IR data set to what can be inferred from calibrated UV/VIS images: the 900, 950, and 1000 nm bands which characterize the 0.85-1 μm Fe^{2+} absorption and the 750 nm band which is considered as representative of the continuum. We used the calibration scheme from the Brown university web site for the absolute UV/VIS data calibration (http://www.planetary.brown.edu/clementine). Absolute residual errors are estimated at the 4% level [*Pieters et al.,* 1994].

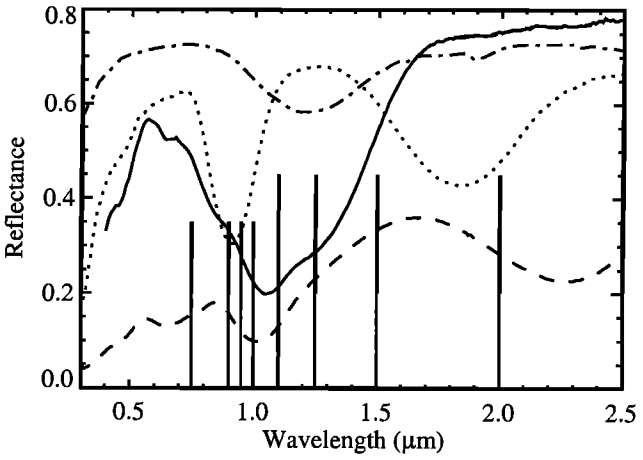

Figure 1. Absolute reflectance spectra of the most common lunar minerals. Clinopyroxene (dashed line), olivine (solid line), orthopyroxene (dotted line), and plagioclase feldspar (dash dotted line) were mesured with RELAB at Brown University. The vertical lines correspond to the center wavelengths of the 8 Clementine filters used in this study.

Our investigations are mainly based on the use of band ratios. This technique is very powerful to highlight and to map the compositional heterogeneity of a surface. Differences in brightness due to illumination conditions are eliminated by the ratio, and variations of the surface reflectance in each wavelengh are the only remaining source of variability in the resulting images. Furthermore, the ratio gives directly the relative variations in band absorption depth, which are in general lower than 15%. A deep absorption feature relative to the surrounding can be interpreted as a high abundance in the mafic minerals. A second possible interpretation is a low content in agglutinate glass, which enhances absorption features in immature soils [*Fischers and Pieters,* 1994, 1996; *Lucey et al.,* 1991a].

Five band ratios were selected to discriminate between orthopyroxene, clinopyroxene, olivine, and plagioclase (see Figure 1). The 950/750 nm ratio is correlated to the Fe^{2+} absorption [*Larson et al.,* 1991], and the 1000/900 nm ratio is used to evaluate if the band center is closer to 900 nm than to 1000 nm, for the discrimination between orthopyroxene and clinopyroxene. The 1100/1500 nm ratio detects absorption due to clinopyroxene and olivine. High contents in plagioclase correspond to high values of this ratio. The 1250/1500 nm ratio is correlated to the abundance of olivine and plagioclase. Finally, the 2000/1500 nm ratio is correlated to the content in pyroxene. The discrimination between olivine and pyroxene is made possible by the use of the NIR domain. While pyroxene exhibits two absorption features in the near infrared at 1 and 2 μm, olivine has a single composite feature centered near 1 μm and has a high reflectance in the 2 μm region. The ratio we present in this paper are all normalized to their mean value, and visualized with a gray scale from 0.7 or 0.8 (black) to 1.2 or 1.3 (white). Absorption relative to the surrounding material can therefore be theoretically evaluated directly in percentage.

3. Systematic Effects in the NIR Images

3.1. Technical Background

The Clementine spacecraft was inserted into an elliptical polar orbit, where it spent 71 days performing a systematic mapping of the Moon. The near infrared camera used a catadioptric lens with an actively cooled 256 x 256 InSb focal plane array (FPA). The FPA operated at 70 K $\pm$0.5 K, with a very good stability over the whole mapping phase [*Priest et al.,* 1995]. The scientific modes implemented four integration times, 32 levels of gain and 256 levels of an analog offset, which was applied before the multiplication by the gain. These working modes have been selected during the mission so as to adjust the signal to the 256 levels dynamic range of the analog to digital camera output. For each orbit, observations of the lunar surface on the dayside were sepa-

rated into 10 latitude segments, during which the gain, offset mode, and integration time for each filter remained constant. A temperature sensor indicated a warming of optics ranging typically from 260 K to 285 K between early (south) and late (north) images during a mapping orbit. A second temperature probe showed a cryocooler warming of about 15° along the orbit, which did not modify the temperature of the detector. Systematic dark frames acquisitions have been performed at the beginning of each orbit by observing space. They were therefore obtained at low temperatures of both the optics and cryocooler.

3.2. Instrumental Effects in the Dark Frame Signal

One of the most challenging features for data interpretation of the NIR data set is the large dark frame signal, which varies with the temperature of the optics (and of the cryocooler) and therefore with time along the orbit. One explanation of this problem has been given by *Priest et al.* [1995] and *Lucey et al.* [1998]: It could be due to a failure of the contact between the cold filter and the cold shield during launch. We made a systematic study of a set of images acquired by observing space with several gain modes, offset modes, and exposure times mainly at the beginning of each mapping orbit, over the south pole, and after the end of the mapping orbit during Earth observations. We derived additional dark frames by selecting zones in shadowed area on images taken at very high or very low latitudes over both the South and the North Poles. The intrinsic noise of the Clementine IR data is lower than 1 digital number (DN) for low signals, as demonstrated by the comparison of successive dark sky observations obtained with the same observation parameters. Dark frames derived from images of the south polar region are also identical to dark frames obtained from observations of the sky within instrumental errors. Dark frames derived from north pole images, when the temperature of the optics and casing are much higher, exhibit signals which can be twice larger than the south dark frames obtained with the same observation parameters. This is confirmed by the few observations of dark sky obtained at northern latitudes. There is therefore a thermal contribution, or correlation, within the dark frame signal. In addition to the thermal background, the changes in the temperature of the electronics may have modified the values of the offset and gain, which are both defined from resistors [*Lucey et al.*, 1998]. Our analysis of the dark frame signal can be summarized by the following list of systematic effects: (1) a fixed pattern of dead pixels with another fixed pattern of defective pixels; (2) a high-frequency column dependent pattern; (3) a pattern of nearly vertical "fringes" with a period of ~30 pixels, which is different for each exposure time; (4) an edge brightening which is correlated with instrument temperature variations; (5) a slightly higher level in the upper half of the CCD; (6) higher levels in the upper left corner which correspond to light emission by the output amplifier [*Martinez and Klotz*, 1997, p. 45] and (7) an offset which may not correspond to the offset described in the "offset_mode" field extracted from the header.

Dark images (from sky observations or reconstructed from dark areas) are not available for all the sets of operating parameters (integration time, offset, gain, instrument temperatures) during the nearly global mapping of the lunar surface. For most images, dark images with the same integration time and gain can be found, whereas the offset mode and instrument temperature can be different or uncertain, as the offset mode from the header is not reliable. As indicated in the introduction, our test regions (Aristillus, Aristarchus, and Kepler) are at low to mid northern latitudes, for which dark frames with the same operating temperatures have been found. The only remaining uncertainty after removing this dark frame is therefore the actual difference in offsets.

4. Reduction Steps Used for the NIR Frames

4.1. Interpolation of Defective Pixels

Each defective pixel detected from abnormally high or low values is replaced by the median value of its neighbors. Approximately 1100 pixels have been typically considered as defective. This represents ~2% of the detector and thus will have a minor contribution in the following steps. No major cluster is present except a square of 2×2 pixels and a vertical line in the lowest part of the matrix. The interpretation of band ratios and extracted spectra will be restricted to areas which have a spatial extent greater than 5x5 pixels. As a consequence, the effect of replacing a defective pixel by the median of its neighbors does not affect the results presented here. In future work, it is planned to use pixels in overlapping frames to replace these pixels. This will require a thorough understanding of the photometric and geometric effects within a frame and between two overlapping frames.

4.2. Dark Frame Subtraction

The next step is the subtraction from each image of a dark frame acquired with the same gain mode, exposure time, and the nearest instrument temperatures. This reduces to a large extent the contribution of the instrumental effects described above, but a global differential offset remains.

4.3. Registration of the Different Filters

In order to resample each NIR frame in the 1100 nm pixel grid, we expanded images to 512×512 pixels. Then we used a correlation method on the lower left corner to evaluate the shift between each frame and the 1100 nm frame. Images have been shifted and then expanded in both the x and y directions to minimize the misregistration effect on corresponding band ratios. The accuracy of this process is 0.5 pixels in offset and better than 0.2% in the scaling factors. Finally, each frame was resampled to the 256×256 pixels. These processing steps assume that all distortion effects are linear. This assumption is correct for viewing geometry effects, as we are dealing with midlatitudes in a near-nadir pointing geometry. Changes in image size due to the possible dependence of the optics focal length with wavelength are also expected to be linear. Therefore, only aberrations introduced by the optics could result in nonlinear effects. The

maximum displacement between two NIR filters is less than 25 pixels, which minimizes these effects. Residual misregistration errors have been checked a posteriori on band ratios. In our images, they are always <0.3 pixels, which introduces a distorsion of the same order as the high-frequency noise of the ratios. In further investigations, we are planning to register images at the 0.2 pixels level instead of 0.5, in particular for high-latitude regions with higher levels of contrast.

4.4. Evaluation of the Differential Offset

Our procedure is based on the relatively small amplitude of spectral variations compared to changes in albedo and illumination. We therefore assume as a first approximation that the surface is spectrally homogeneous, so that the 750 nm and IR signals are proportional. The procedure includes two main steps. First, the decalibrated 750 nm image is resampled to the 1100 nm pixel grid. This implies shifting, expanding, and rotating the 750 nm image. Rotation is not necessary among the NIR frames nor among the UV/VIS ones. But rotation is needed for coregistration between NIR and UV/VIS sets. The algorithm used to resample the rotated frames is the nearest neighbors. This method conserves flux with a maximum error of 0.2%.

After subtraction of the dark frame, we have, assuming spectral homogeneity:

$$[750\text{ nm}] = k\frac{[\text{NIR}] + \text{offset}}{\text{flat}_{\text{NIR}}} \quad (1)$$

where flat_{NIR} is the flat field which has been resampled to the 1100 nm pixel grid with the same parameters as the corresponding NIR image. Both k and the differential offset can therefore be determined from a linear regression correlation between each NIR image and the resampled 750 nm image multiplied by the resampled IR flat field (see Figure 2). The determination of NIR flat fields is described below. In specific cases, band ratios reveal that major spectral heterogeneities occur within the area used for the offset determination. In such cases, the evaluation of the offset is restricted to a spectrally homogenous area. We made the assumption that the UV/VIS data is properly calibrated. However, residual stray light problems have been identified from observations near the lunar limb. Stray light reduces the contrast of the image by adding a slowly varying contribution. This effect contributes to the 4% overall uncertainty on UV/VIS data. As a result, the IR offsets can be overestimated by up to 8 DN. However, as the same UV/VIS filter is used as a reference for the four NIR filters, the errors in the offsets are strongly correlated so that there is only a second-order effect on band ratios. After normalization, the induced error on band ratios is <1.5% even in dark regions, a factor of 2 smaller than the high-frequency variance of the band ratios and a factor of 10 smaller than the largest low-frequency variations, which result from heterogeneities in mineralogy and/or maturity.

4.5. Division by the Flat Field

The NIR flat fields have been derived for each filter from a set of 17 images of Mare Imbrium obtained within a 10° latitude bin. These images are relatively homogeneous except for small fresh craters with immature bright ejectas. Dark frames obtained during mispointed observations of the Earth are available for each filter with the same gain and integration time and with differences in instrument temperatures smaller than two degrees. The dark frame was sub-

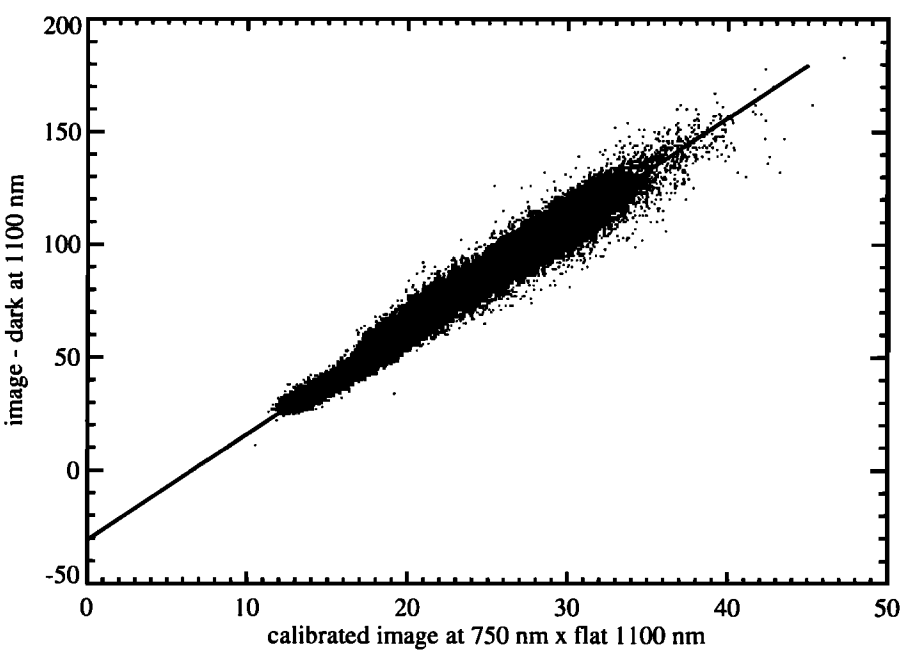

Figure 2. Correlation plot of the Aristarchus 1100 nm data versus the calibrated and resampled UV/VIS 750 nm data multiplied by the 1100 nm NIR flat field. The linear correlation between the two data sets is used to determine the offset.

tracted from each image, then the dead or defective pixels were eliminated. A first evaluation of the differential offsets was made using the procedure described above, assuming a perfectly homogeneous flat field. The median of the 17 values for each pixel was selected as representative of a uniformly illuminated image, by eliminating in particular the small bright crater ejectas. The flat field was obtained by normalizing the result to the mean value. A recursive process was performed with this first flat fields evaluation to refine the differential offsets between Mare Imbrium images and corresponding darks frames and thus to improve the evaluation of a second set of more accurate flat fields.

Equation 2 summarizes the reduction process for NIR frames:

$$\text{image} = (\text{raw} - \text{dark} + \text{offset})/\text{flat}_{\text{NIR}} \quad (2)$$

were offset, and flat_{NIR} are derived from the procedures described above. The reduction process leaves an unknown multiplicative factor for each frame, which includes in particular the gain, the integration time and the effective width of each filter. In order to eliminate this unknown factor, band ratios are normalized to unity, and extracted spectra are scaled with a telescopic spectrum as ground truth.

5. Checks of the Accuracy of the Method

As a first test, we applied our offset determination method to the UV/VIS images at 0.9, 0.95, and 1 μm. We obtained offsets consistent with those derived from the header and the calibration procedure with an accuracy of 1 DN. The linear relationship between different spectral bands is therefore a valid first-order approximation. We have also checked the validity of the evaluated global offset on band ratios. If there is an error on the offset of one of the NIR images, the band ratio will show a correlation with illumination within mineralogically homogeneous zones. Finally, the offset determination has also been tested using correlation computation within the NIR data cube itself to confirm the self consistency of the values. With these tests, we estimate the accuracy of the offset determination method to be better than 4 DN for the NIR frames with a given flat field.

The accuracy of the whole data reduction process has been checked by comparing spectra and band ratios in overlaping zones of adjacent frames. Nearly a third of the NIR field of view is observed twice in two successive frames. This overlap is very useful to check the consistency of the reduction process. After the whole calibration scheme, the band ratios in the overlaping zones are supposed to be exactly the same in both frames. The dispersion on a band ratio is estimated at a level of $\sim$3% after these processing steps.

6. Results

We focused our analysis on lunar zones which are expected to show a compositional heterogeneity. Craters large enough to have a central peak have excavated materials of the lunar crust from a depth of several kilometers [*Roddy*, 1977; *Dence et al.*, 1977]. Central peaks are therefore of major interest to find materials which spectrally differ from the surroundings. From another point of view, the maturity of lunar soils reduces spectral contrast [*Fischers and Pieters*, 1994, 1996; *McKay et al.*, 1991, p. 309]. The degree of maturity of the soil is directly linked to the period of time a soil has been exposed to space weathering. The main space weathering processes are the bomdardment by micrometeorites, solar wind ions, and solar flare particles. The spectral characteristics of a mature lunar soil are a reduced global reflectance, a reduced absorption band depth, and an increased slope of the continuum. Relatively young craters give access to soils which are more immature and exhibit deeper absorption features. We therefore focused our attention on three different areas, which are the Aristillus, Aristarchus, and Kepler craters. The frame numbers of all NIR images used in this paper are listed in Table 1.

The 55 km diameter crater Aristillus is located at 33.9°N and 1.2°E on the eastern part of Mare Imbrium. A previous telescopic study of the crater has been made by *Smrekar and Pieters* [1985]. We computed a mosaic of two adjacent frames (Figure 3) using our selection of UV/VIS and NIR data. The two band ratio images are very similar in the overlapping region, validating our flat field and offset evaluation. The landing site of Apollo 15 is located at about 250 km on the south of Aristillus. The impact event forming Aristillus could be the origin of some samples returned by the Apollo 15 mission. The lunar sample 15405 in particular is thought to be part of the ejectas from this crater [*Spudis and Pieters*, 1991, p. 622].

An analysis of the color ratio displayed in Figure 3 gives important information on the crater mineralogy. A good correlation exists between the 2000/1500 nm and the 950/750 nm ratios, indicating either a high pyroxene content in the central peak complex (arrows a), and in several parts of the rim, or a very immature soil. The problem of distinguishing between the optical effects due to exposure and those due to composition is discussed by *Fischers and Pieters* [1994,

Table 1. List of the NIR Frame Numbers Used in This Study

Feature	Images	Images	Darks
Aristillus	lna3395m.168	lna3364m.168	lna5951y.191
	lnb3410m.168	lnb3379m.168	lnb5766y.193
	lnc3402m.168	lnc3371m.168	lnc5518p.102
	lnd3407m.168	lnd3376m.168	lnd3430d.231
Aristarchus	lna2981l.186	lna2950l.186	lna1968y.326
	lnb2996l.186	lnb2965l.186	lnb6082y.275
	lnc2988l.186	lnc2957l.186	lnc5600y.166
	lnd2993l.186	lnd2962l.186	lnd2079y.326
Kepler	lna3724j.050		lna5951y.191
	lnb3739j.050		lnb5766y.193
	lnc3731j.050		lnc5518p.102
	lnd3736j.050		lnd5713y.196

File naming conventions: l=lunar mapping; n=near infrared sensor; a, b, c, and d= filters at 1100, 1250, 1500, and 2000 nm respectively; last letter= latitude bin; last 3 digits= orbit number.

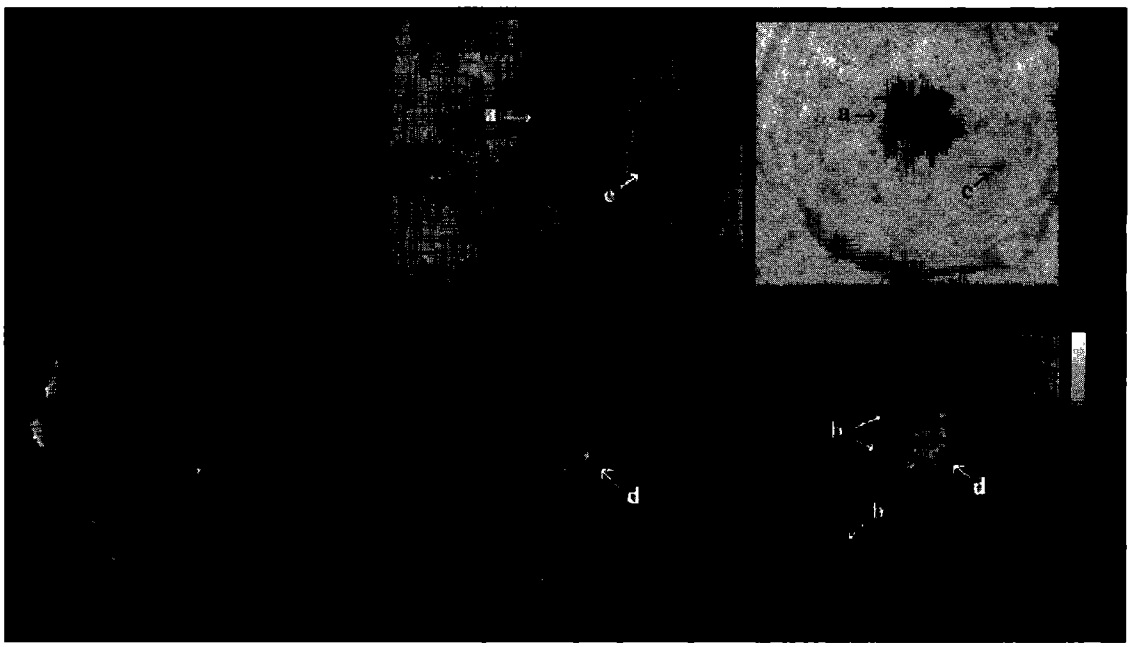

Figure 3. Band ratios on aristillus. Pyroxene dominated central peak (arrow a), high-Ca clinopyroxene rich regions (arrow b), small fresh crater (arrow c), and low-Ca orthopyroxene rich region in the central peak (arrow d) are shown. North is on the left.

1996] and *Lucey et al.* [1991b]. As there is no strong correlation with albedo, nor with other ratios, we believe that the high pyroxene content is the most plausible hypothesis for the central peak of Aristillus. A strong anticorrelation with albedo would have indicated a low degree of maturity rather than a different composition. The average composition of the pyroxene can be estimated using the wavelengh of the 1 μm band center [*e.g., Adams*, 1974]. Low-Ca orthopyroxene has a band centered at 0.91 μm while a higher Ca content shifts the band center to 0.99 μm for clinopyroxene. As a consequence, the 1000/900 nm ratio discriminates between orthopyroxene and clinopyroxene components. This ratio revealed a high clinopyroxene content in the northern part of the peak and the north western part of the rim (see arrows b in Figure 3). Both 1250/1500 nm and 1100/1500 nm ratios are noisier but appear very homogeneous, excluding pure plagioclase or very high contents in olivine. High values of the 1250/1500 nm ratio in the southern part of the central peak complex are consistent with the presence of orthopyroxene (arrow d). Arrow c in Figure 3 indicates a small fresh crater, which has excavated more immature material dominated by pyroxene. Spectra have been extracted from zones of particular interest.

Telescopic spectra have been acquired by *Smrekar and Pieters* [1985] on two locations within our mapping zone and are located respectively on the northern rim (a4) and the central peak (c3) of the crater. Spectral calibration is obtained by scaling our data cube to the telescopic spectrum of Aristillus labeled a4. Spectra of different parts of the frame were then extracted to estimate the compositional heterogeneity of the crater. The location of the selected zones are displayed in Figure 4. These reflectance spectra are scaled to unity at 1.0 μm and are offset for clarity (see Figure 5a). In order to emphasize weak absorption features, spectra are also divided by a straight line fitting the spectrum at 0.75 and 1.5 μm, considered to be representative of the steeply sloped continuum (see Figure 5b).

We checked the validity of our approach by comparing the second telescopic spectrum labeled c3 from *Smrekar and Pieters* [1985] with the NIR spectrum extracted from the same zone on the central peak (see Figure 6). A good agreement is obtained between both data sets.

Although the spectral resolution is too low for a very accurate study of mineralogical components, distinct features

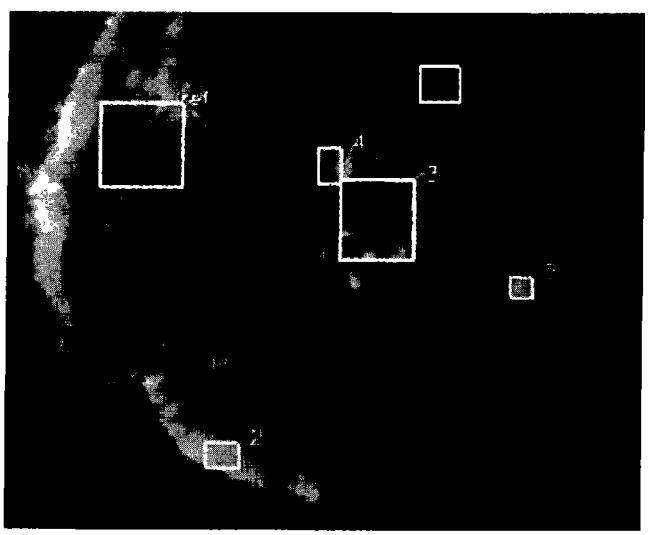

Figure 4. Location of spectra extracted from Aristillus area. North is on the left.

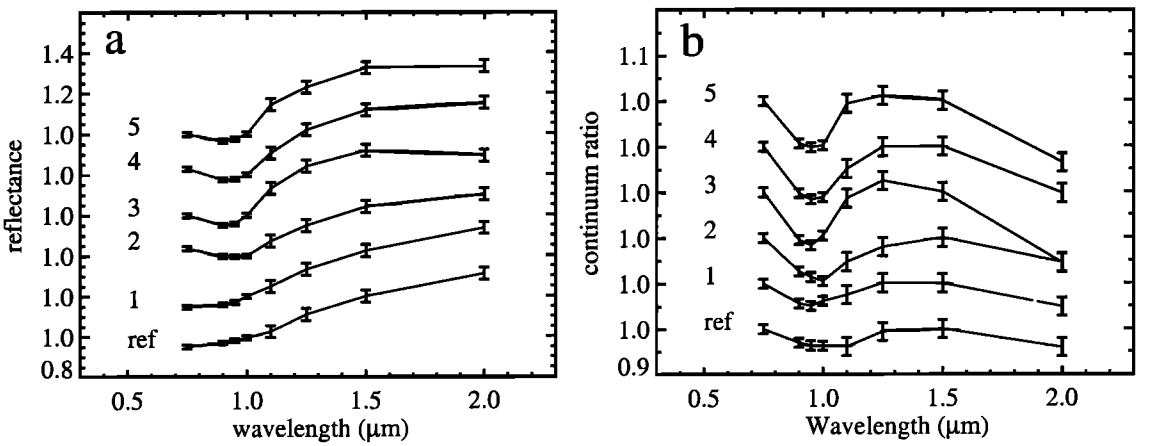

Figure 5. Reflectance spectra extracted from Aristillus (see locations in Figure 4). (a) Reflectance spectra have been scaled to unity at 1.0 μm. (b) Spectra divided by a continuum as described in the text.

are clearly apparent on the five extracted spectra. The crater floor (spectrum 1 in Figure 5) exhibits spectral characteristics very similar to the reference zone. This kind of spectrum has been interpreted by *Smrekar and Pieters* [1985] as a mixture of pyroxene with a Fe-bearing glass or a feldspar. The north western inner part of the rim (arrow b on the rim in Figure 3 and spectrum 2 in Figure 5) exhibits spectral features which are consistent with a high content in clinopyroxene. The derived spectra from the central peak (spectra 3 and 4 in Figure 5) are in good agreement with the corresponding telescopic spectrum of *Smrekar and Pieters* [1985], which was interpreted as a mixture of high and low Ca pyroxenes or as a pyroxene of intermediate Ca content. The band ratios shown in Figure 3 are consistent with this interpretation, and show the spatial distribution of the pyroxene on the central peak. The telescopic spectrum of *Smrekar and Pieters* [1985], which included almost all the central peak, could be therefore explained as the result of a linear spectral mixing of clinopyroxene (northern part of the peak, arrow b, and spectrum 4 in Figure 3) and orthopyroxene (arrow d in the southern part of the peak). Finally, a fresh crater on the floor of Aristillus (see arrow c in Figure 3 and spectrum 5 in Figure 5) also exhibits spectral characteristics consistent with high pyroxene content. The low degree of maturity of this small crater can be inferred from its very high albedo. A less mature, recently excavated material could then explain the sharper absorption feature at 1 and 2 μm.

In order to permit comparison with previous studies of Clementine NIR data, we computed a mosaic of two adjacent frames of the relatively fresh Copernician crater Aristar-

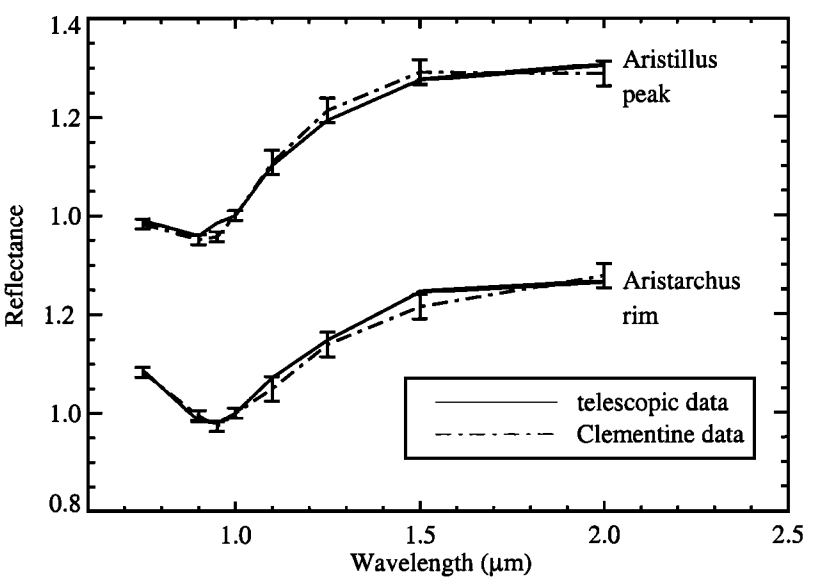

Figure 6. Comparison between NIR data and telescopic spectra. For Aristillus, we used spectrum a4 from *Smrekar and Pieters* [1985] for calibration. A good agreement between their spectrum c3 and our Clementine spectrum is found on the central peak. For Aristarchus, we used spectrum 2a from *Lucey et al.* [1986] for the calibration. Their spectrum 1c of the rim is also consistent with the corresponding Clementine spectrum of the same zone.

chus. Aristarchus is 40 km in diameter and is located at 23.7°N 313°E. Several telescopic studies of the crater and the surrounding region have been made [*Lucey et al.*, 1986; *Pinet et al.*, 1996], showing a global heterogeneity of the surface. A small olivine rich area on the south crater rim and anorthositic central peaks have been previously reported by *McEwen et al.* [1994], using preliminary interpretations of the NIR data. Our results are in good agreement with these conclusions (see arrows a and b in Figure 7). Our improved registration and the spatial extent due to the mosaicking reveals additional details. However, it should be noted that the central peaks are nearly saturated on the 1250 nm image, which casts some doubts on the conclusion about the anorthositic component. Our spectra have been extracted from the data using the telescopic spectrum 2a of *Lucey et al.* [1986] as a reference (Figures 8 and 9).

We tested the accuracy of the reduction process by extracting a spectrum from area 1 in Figure 8 and by comparing it with the corresponding telescopic spectrum 1c from *Lucey et al.* [1986]. Both spectra are in good agreement (see Figure 6).

The rim of the crater is not conspicuous on the 1100/1500 nm and on the 1250/1500 nm ratio. It appears more clearly with low values on the 2000/1500 nm ratio, with a good correlation with the 950/750 nm ratio. The upper part of the rim exhibits the lowest values in the 2000/1500 nm ratio. Spectrum number 2 in Figure 5 exhibits the deepest absorption at 2 μm compared to the other spectra, suggesting a major pyroxene component. Two small areas (arrows a in Figure 7) exhibit low values for both the 1100/1500 nm and the 1250/1500 nm ratios and high values for the 2000/1500 nm ratio. Furthermore, the two areas have a low albedo. This is consistent with a high olivine content as previously reported for one of the two areas by *McEwen et al.* [1994]. Spectra from the corresponding zones (3 and 4 in Figure 8) have been extracted. Their 1 μm absorption feature confirms a large abundance of olivine (Figure 9). Spectra of mixtures containing 75% of olivine with 25% of pyroxene made by *Singer* [1981] match the observed shape of spectrum 3. It is very interesting to notice that the UV/VIS part of the spectra is very similar in each scanned zone. On the contrary, the NIR domain contains crucial information which makes possible the discrimination between pyroxene and olivine. Furthermore, units mainly dominated by olivine are rarely detected on the lunar surface, whereas olivine is known to be a common component of the maria. The central peaks of Copernicus have been reported to be dominated by olivine [*Pieters*, 1982; *Lucey et al.*, 1991b]. This observation supports the idea that the lower crust and possibly the lunar mantle itself could be at a shallow depth in this area [*Pieters and Wilhelms*, 1985; *Pinet et al.*, 1993]. In order to constrain this hypothesis, we computed band ratios on Kepler, a smaller crater located only 500 km to the East of Copernicus.

The relatively young Copernician crater Kepler is located on the south of Mare Imbrium at 8.1°N 37.9°W and is 32 km in diameter. A bright system of emerging rays indicates a low degree of maturity of the excavated material. Band ratios are displayed in Figure 10. The UV/VIS part is a mosaic of two adjacent frames whereas the NIR part is a single frame. A very good correlation is observed between the 2000/1500 nm and the 950/750 nm ratios, suggesting either a high content in pyroxene or a very immature soil. The whole crater rim appears in low values (dark) in both cases. On the contrary, the rim appears as slightly high values in

Figure 7. Band ratios on Aristarchus crater. Small olivine rich areas on the rim (arrows a) and anorthositic peaks (arrow b) are shown. North is on the left.

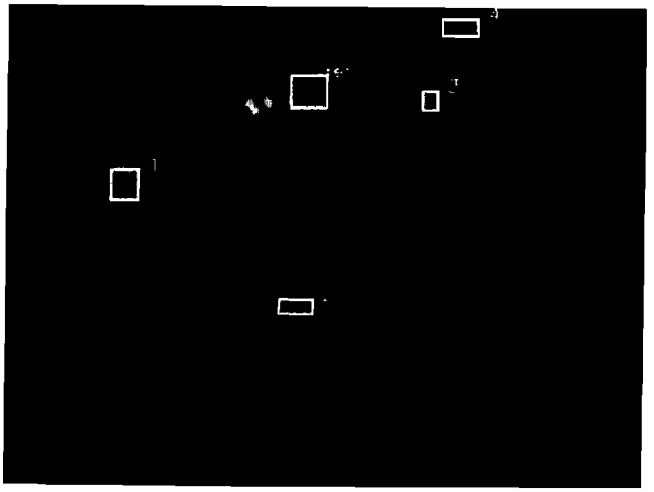

Figure 8. Location of spectra extracted from Aristarchus area. North is on the left.

both 1100/1500 nm and 1250/1500 nm ratios. The discrimination between a maturity effect and a composition effect is more ambiguous than for the Aristillus case, as the system of very bright rays attests the relative young age of the crater. However, no obvious correlation exists between albedo and any of the ratios. The upper left corner of the rim almost disappears in ratios whereas it is still present in the albedo frame. The lower part of the rim exhibits low values of both 2000/1500 nm and 950/750 nm ratios but shows no obvious albedo pattern. We therefore conclude that both immaturity and compositional heterogeneity effects are present. Band ratios are consistent with a noritic composition. The steep slopes of the crater inner rim could explain the sharpness of the absorption features by exposing less mature material. According to the aspect of band ratios, the central peak does not differ markedly from the surrounding regions. This indicates that the central uplift of fractured, shocked target rock material, which could come from a depth of 3 to 6 km, has the same mineral composition as the local upper crust. No major olivine occurence is detected. The diameter of Kepler is one third of the diameter of Copernicus. The Kepler impact was not large enough to excavate the possible underlying olivine-rich unit, as was the case for Copernicus.

7. Summary and Conclusion

This work shows the great potential of the Clementine NIR data set for lunar mineralogy. Our attention has been focused on the data reduction process for selected areas of the Moon, using calibrated UV/VIS images as a reference for offsets determination. Flat fields have been extracted from the data set itself using a median filter on selected homogeneous images of Mare Imbrium. In order to limit the changes in instrumental behavior observed with increasing cryocooler and lens temperatures along the orbit, we selected three craters located at low-latitudes to midlatitudes on the border of Mare Imbrium: Aristillus, Aristarchus, and Kepler. We computed band ratios to map the compositional heterogeneity, and we extracted spectra using two telescopic spectra as reference. The distribution of the high and the low Ca pyroxene has been mapped on Aristillus. The central peak complex exhibits features suggesting a high content in both clinopyroxene and orthopyroxene. Spectra consistent with mixtures containing >75% olivine and <25% pyroxene have been found on the south rim of Aristarchus. Finally, a very deep absorption at 2 μm has been detected on the rim of Kepler, correlated with a very strong 1 μm absorption, suggesting either a high content in orthopyroxene or a very immature soil. The NIR data set contains information which are of great interest in improving our knowledge of the lunar mineralogy.

After this first investigation, much work is still needed to fully exploit the potential of the NIR data set. The calibration effort by the PI team should provide improved calibration parameters for the NIR channel in the near future. The next major steps which we consider for our approach are first to improve the dark current and flat field corrections for

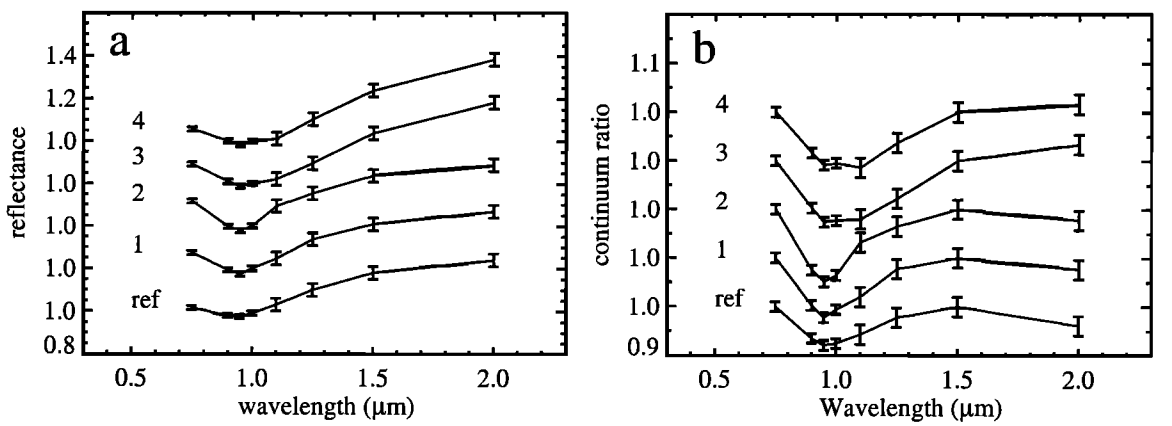

Figure 9. Reflectance spectra extracted from Aristarchus (see locations in Figure 8). (a) Reflectance spectra have been scaled to unity at 1.0 μm. (b) Spectra divided by a continuum as described in the text are displayed. Spectra 3 and 4 suggest a very high content in olivine.

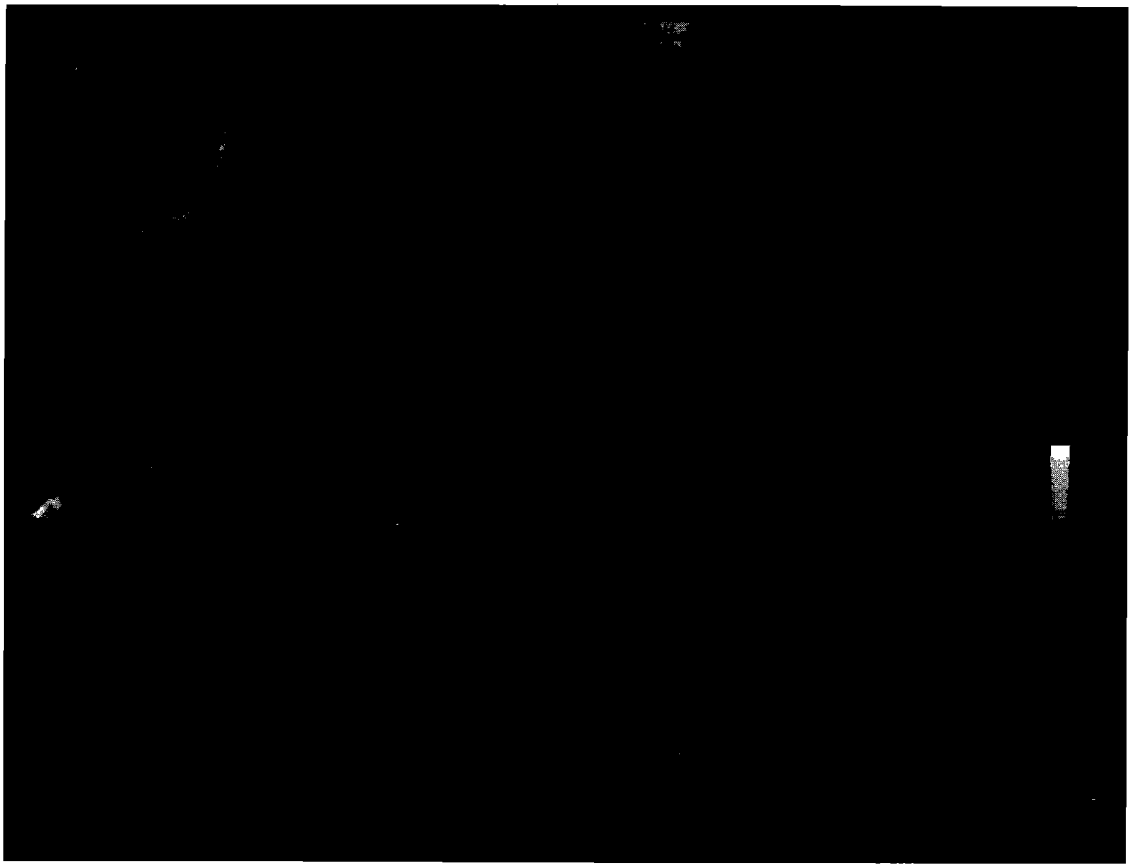

Figure 10. Band ratios on Kepler. A very good correlation exists between 2000/1500 nm and 950/750 nm ratios, suggesting the presence of pyroxene on the crater rim. North is on the left.

each of the four filters which have already been investigated and to study the possible dependence on the integration time. We also plan to extend our approach to the other two filters, taking into account the thermal component at 2.76 μm. In this contribution, we have restricted our analysis to regions with small variations of the relevant temperatures (optics and cryocooler, the latter being most likely related to the temperature of the electronics). We are also planning to take into account photometric corrections within each frame and from one frame to the next. This will allow us to extend our results to regions at very different latitudes. With these improvements, our bootstrapping approach should be useful as a test of the remaining uncertainties on the calibration parameters once they are made available by the PI team.

Acknowledgments. The authors are grateful to P. G. Lucey for a useful discussion during the 29th LPSC. We also would like to thank P. Johnson and an anonymous reviewer for their very helpful comments and suggestions.

References

Adams, J. B., Visible and near-infrared diffuse reflectance spectra of pyroxenes as applied to remote sensing of solid objects in the solar system, *J. Geophys. Res., 79*, 4839-4836, 1974.

Cloutis, E. A., and M. J. Gaffey, Lunar regolith analogues: Spectral reflectance properties of compositional variations, *Icarus, 102*, 203-224, 1993.

Crown, D. A., and C. M. Pieters, Spectral properties of plagioclase and pyroxene mixtures and the interpretation of lunar soil spectra, *Icarus, 72*, 492-506, 1987.

Dence, M. R., R. A. F. Grieve, and P. B. Robertson, Terrestrial impact structures: Principal characteristics and energy considerations, in *Impact and Explosion Cratering*, edited by D. J. Roddy, R. O. Pepin, and R. B. Merill, pp. 247-276, Pergamon, Tarrytown, New York, 1977.

Fischers, E. M., and C. M. Pieters, Remote determination of exposure degree and iron concentration of lunar soils using VIS-NIR spectroscopic methods, *Icarus, 111*, 475-488, 1994.

Fischers, E. M., and C. M. Pieters, Composition and exposure age of the apollo 16 Cayley and Descartes regions from Clementine data: Normalizing the optical effects of space weathering, *J. Geophys. Res., 101*, 2225-2234, 1996.

Isbell, C. E., E. M. Eliason, T. Becker, E. M. Lee, A. McEwen, and M. Robinson,The Clementine mission: An archive of a digital image model of the Moon, *Lunar Planet. Sci., XXVIII*, 623-624, 1997.

Larson, S. M., J. R. Johnson, and R. B. Singer, Evaluation of the sensitivity of the reflectance ratios to mafic minerals in the lunar regolith, *Geophys. Res. Lett., 18*, 2149-2152, 1991.

Lucey, P. G., B. R. Hawke, T. B. McCord, C. M. Pieters, and J. W. Head, A compositional study of the aristarchus region of the moon using near-infrared reflectance spectroscopy, *J. Geophys. Res., 82*, D344-D354, 1986.

Lucey, P. G., B. R. Hawke, and K. Horton, Visible and infrared imaging of Copernicus crater and surroundings, *Lunar Planet. Sci., XXII*, 833-834, 1991a.

Lucey, P. G., B. R. Hawke and K. Horton, The distribution of olivine in the crater Copernicus, *Geophys. Res. Lett., 18*, 2133-2136, 1991b.

Lucey, P. G., J. L. Hinrichs, and E. Malaret, Progress toward calibration of the clementine NIR camera data set, *Lunar Planet. Sci., XXVIII*, 843-844, 1997.

Lucey, P. G., et al., Calibration of the Clementine near infrared camera: Ready for prime time, *Lunar Planet. Sci., XXIX*, 1576-1577, 1998.

Martinez, P., and A. Klotz, *A Practical Guide to CCD Astronomy.*, Cambridge Univ. Press, New York, 1997.

McEwen, A. S., M. S. Robinson, E. M. Eliason, P. G. Lucey, T. C. Duxbury, and P. D. Spudis, Clementine observations of the aristarchus region of the moon, *Science, 266*, 1858-1862, 1994.

McKay, D. S., G. Heiken, A. Basu, G. Blanford, S. Simon, R. Reedy, B. M. French and J. Papike, The lunar regolith, in *Lunar Sourcebook*, edited by G. H. Heiken, D. T. Vaniman, and B. M. French, pp. 285-356, Cambridge Univ. Press, New York, 1991.

Nozette, S., et al., The Clementine mission to the Moon: Scientific overview, *Science, 266*, 1835-1839, 1994.

Pieters, C. M., Copernicus crater central peak: Lunar mountain of unique composition, *Science, 215*, 59-61, 1982.

Pieters, C. M., Composition of the lunar highland crust from near-infrared spectroscopy, *Rev. Geophys., 24,* 557-578, 1986.

Pieters, C. M., and D. E. Wilhelms, Origin of Olivine at Copernicus, *J. Geophys. Res., 90*, 415-420, 1985.

Pieters, C. M., M. I. Staid, E. M. Fischer, S. Tompkins, and G. He, A sharper view of impact craters from Clementine data, *Science, 266*, 1844-1848, 1994.

Pinet, P. C., S. Chevrel, and P. Martin, Copernicus- A regional probe of the lunar interior, *Science, 260*, 797-801, 1993.

Pinet, P. C., P. Martin, F. Costard, S. Chevrel, Y. Daydou, and P. E. Johnson, Aristarchus plateau: Clementine spectro-imaging and geological inferences, *Lunar Planet. Sci., XXVII*, 1037-1038, 1996.

Priest, R. E., I. T. Lewis, N. R. Sewall, H. S. Park, M. J. Shannon, A. G. Ledebuhr, L. D. Pleasance, M. A. Massie, and K. Metschuleit, Near-infrared camera for the Clementine mission, *Proc. Int. Soc. Opt. Eng., 2475,* 393-404, 1995.

Roddy, D. L., Large-scale impact and explosion craters: Comparisons of morphological and structural analogs, in *Impact and Explosion Cratering*, edited by D. J. Roddy, R. O. Pepin, and R. B. Merill, pp. 185-246, Pergamon, Tarrytown, New York, 1977.

Singer, R. B., Near-infrared spectral reflectance of mineral mixtures: Systematic combinations of pyroxenes, olivine, and iron oxides, *J. Geophys. Res., 86*, 7967-7982, 1981.

Smrekar, S., and C. M. Pieters, Near-infrared spectroscopy of probable impact melt from three large lunar highland craters, *Icarus, 63*, 442-452, 1985.

Spudis, P., and C. Pieters, Global and regional data about the Moon, in *Lunar Sourcebook*, edited by G. H. Heiken, D. T. Vaniman, and B. M. French, pp. 595-632, Cambridge Univ. Press, New York, 1991.

S. Erard, Y. Langevin, and S. Le Mouélic, Institut d'Astrophysique Spatiale, CNRS-Université Paris XI, Bât 121, 91405 Orsay, France. (erard@ias.fr; langevin@ias.fr; lemoueli@ias.fr)

(Received June 23, 1998; revised October 30, 1998;
accepted November 11, 1998.)